

Correction-to-scaling exponent for percolation and the Fortuin–Kasteleyn Potts model in two dimensions

Yihao Xu,^{1,*} Tao Chen,^{2,†} Zongzheng Zhou,^{3,‡} Jesús Salas,^{4,5,§} and Youjin Deng^{1,2,6,¶}

¹*Department of Modern Physics, University of Science and Technology of China, Hefei, Anhui 230026, China*

²*Hefei National Research Center for Physical Sciences at the Microscale, University of Science and Technology of China, Hefei 230026, China*

³*School of Mathematics, Monash University, Clayton, Victoria 3800, Australia*

⁴*Universidad Carlos III de Madrid, Departamento de Matemáticas, Avenida de la Universidad 30 (edificio Sabatini), 28911 Leganés (Madrid), Spain*

⁵*Grupo de Teorías de Campos y Física Estadística,*

Instituto Gregorio Millán, Universidad Carlos III de Madrid,

Unidad Asociada al Instituto de Estructura de la Materia, CSIC, Serrano 123, 28006 Madrid, Spain

⁶*Hefei National Laboratory, University of Science and Technology of China, Hefei 230088, China*

(Dated: November 18, 2024)

The number n_s of clusters (per site) of size s , a central quantity in percolation theory, displays at criticality an algebraic scaling behavior of the form $n_s \simeq s^{-\tau} A(1 + Bs^{-\Omega})$. For the Fortuin–Kasteleyn representation of the Q -state Potts model in two dimensions, the Fisher exponent τ is known as a function of the real parameter $0 \leq Q \leq 4$, and, for bond percolation (the $Q \rightarrow 1$ limit), the correction-to-scaling exponent is derived as $\Omega = 72/91$. We theoretically derive the exact formula for the correction-to-scaling exponent $\Omega = 8/[(2g+1)(2g+3)]$ as a function of the Coulomb-gas coupling strength g , which is related to Q by $Q = 2 + 2\cos(2\pi g)$. Using an efficient Monte Carlo cluster algorithm, we study the $O(n)$ loop model on the hexagonal lattice, which is in the same universality class as the $Q = n^2$ Potts model, and has significantly suppressed finite-size corrections and critical slowing-down. The predictions of the above formula include the exact value for percolation as a special case, and agree well with the numerical estimates of Ω for both the critical and tricritical branches of the Potts model.

I. INTRODUCTION

Bond percolation [1, 2] is a fundamental model in statistical mechanics, studying the formation and behavior of connected clusters in a lattice as a function of the probability $p \in [0, 1]$ of each edge being occupied. In percolation, a key quantity is the size distribution $n_s(p)$, which gives the number of clusters (per volume) containing s sites. Here, we are concerned with its behavior at the critical point p_c [3]

$$n_s(p_c) = A s^{-\tau} \left(1 + B s^{-\Omega} + \dots \right). \quad (1)$$

where the dots stand for higher-order contributions. The Fisher exponent τ is universal, and takes the value $\tau = 187/91$ in two-dimensional (2D) bond percolation. The correction-to-scaling exponent Ω is also expected to be universal, and its value was precisely determined to be $72/91$ in a recent study [4] (see also Refs. [5, 6]).

Percolation can be defined on any d -dimensional lattice. However, in this paper we will focus on 2D lattices. More specifically, we will consider models defined on finite (undirected) graphs $G = (V, E)$ with vertex (or site)

set V , and edge set E . In statistical mechanics, these graphs are usually taken as finite subsets of a regular 2D lattice with some prescribed boundary conditions [e.g., toroidal in Monte Carlo (MC) simulations]. Therefore, the second-order phase transitions undergone by these models will be governed in the infinite-volume limit by a certain conformal field theory (CFT) [7].

Building on the percolation model, the random-cluster (RC) model [8] introduces a more generalized framework. This model extends percolation theory by assigning a real weight $Q \geq 0$ to each connected cluster, including isolated sites. The partition function for the RC model on a finite graph $G = (V, E)$ is given by

$$Z_{\text{RC}}(G; Q, p) = \sum_{F \subseteq E} p^{|F|} (1-p)^{|E|-|F|} Q^{k(F)}, \quad (2)$$

where the sum is over all spanning subgraphs (V, F) of G , $|F|$ represents the number of occupied edges, $|E|$ is the total number of edges, and $k(F)$ is the number of connected clusters. This model not only generalizes the percolation model (retrieved when $Q = 1$), but is also related to other significant statistical-mechanical models.

The most famous connection is the Q -state Potts model [9–13], a widely studied model in statistical physics, and whose exact solution is still missing. In this model, each spin σ_i , located at a site $i \in V$ of the graph G , takes $Q \geq 2$ possible states, i.e., $\sigma_i \in \{1, 2, \dots, Q\}$. In this setup, Q is an integer parameter. The Hamiltonian

* yhxu@mail.ustc.edu.cn

† taochen@mail.ustc.edu.cn

‡ eric.zhou@monash.edu

§ jsalas@math.uc3m.es

¶ yjdeng@ustc.edu.cn

of this model is given by

$$-\beta \mathcal{H}_{\text{Potts}}(\sigma) = J \sum_{\{ij\} \in E} \delta_{\sigma_i, \sigma_j}, \quad (3)$$

where σ_i and σ_j represent the states of neighboring sites i and j , $\delta_{a,b}$ is the Kronecker delta function, β is the inverse temperature, and $J \in \mathbb{R}$ is the reduced nearest-neighbor coupling. Here we will consider the ferromagnetic regime of this model $J > 0$. Its partition function in this spin representation is given by

$$Z_{\text{Potts}}(G; Q, J) = \sum_{\{\sigma\}} e^{-\beta \mathcal{H}_{\text{Potts}}(\sigma)}, \quad (4)$$

where the sum is over all possible spin configurations $\{\sigma\}$.

This partition function (4) can be rewritten in the so-called Fortuin–Kasteleyn (FK) [14, 15] representation as

$$Z_{\text{Potts}}(G; Q, v) = \sum_{F \subseteq E} v^{|F|} Q^{k(F)}, \quad (5)$$

where the sum is over all spanning subgraphs (V, F) of the graph G , $Q \geq 2$ is an integer, and the temperature-like variable $v = e^J - 1$ belongs to the physical interval $v \in [0, \infty)$ in the ferromagnetic regime. Due to the fact that (5) is a polynomial jointly in Q and v , we can promote these two variables from their physical ranges to arbitrary real, or even complex variables. In particular, if $Q, v > 0$, the model (5) has a probabilistic interpretation. The RC model (2) with $p = v/(1+v)$ directly maps onto the FK representation of the Potts model (5), modulo some uninteresting prefactors.

The Potts model (3)/(4) can be generalized to include vacancies: these are basically integer variables $\tau_i \in \{0, 1\}$ living on the sites of the graph, and such that $\tau_i = 0$ (resp. $\tau_i = 1$) means that the site $i \in V$ is empty (resp. occupied). A simple Hamiltonian of this kind is given by [10, 16, 17]

$$-\beta \mathcal{H}_{\text{dPotts}}(\sigma, \tau) = \sum_{\{i,j\} \in E} \tau_i \tau_j (K + J \delta_{\sigma_i, \sigma_j}) - \Delta \sum_{i \in V} \tau_i, \quad (6)$$

where Δ is the chemical potential governing the concentration of vacancies. The corresponding partition function is

$$Z_{\text{dPotts}}(G; Q, J, K, \Delta) = \sum_{\{\sigma, \tau\}} e^{-\beta \mathcal{H}_{\text{dPotts}}(\sigma, \tau)}, \quad (7)$$

where the sum is over all possible spin $\{\sigma\}$ and vacancy $\{\tau\}$ configurations. Other similar Hamiltonians have been considered in the literature [18–22]. The diluted Potts model (6) appears naturally when performing a real-space renormalization-group (RG) transformation on the “pure” Potts model [16, 17]. The number of states Q does not renormalize; it stays constant along any RG trajectory. On the critical surface for $Q \in [0, 4]$, there is a line of (attractive) critical fixed points (in the same universality class as the original Potts model), and there is

another line of (repulsive) tricritical fixed points (belonging to a distinct universality class as its critical counterpart). Both lines meet at $Q = 4$. For $Q > 4$, the system renormalizes to a discontinuity fixed point (at zero temperature), as expected [23–25].

Many critical exponents for the original and diluted Q -state Potts models for $Q \in [0, 4]$ are well known. One way of obtaining such exponents is by relating both models to a Coulomb gas (CG) [26, 27] with a certain coupling constant g (whose definition is not universal in the literature). In this paper, the parameters Q and g are related via

$$\sqrt{Q} = -2 \cos(\pi g), \quad g \in \left[\frac{1}{2}, 2\right]. \quad (8)$$

Both the critical and tricritical lines are covered by this parametrization: the interval $g \in [1/2, 1]$ (resp. $g \in [1, 2]$) corresponds to the critical (resp. tricritical) line. Indeed, at $Q = 4$ (or $g = 1$) both lines merge.

The leading and subleading thermal exponents y_{t1} and y_{t2} relate to g as (see e.g., Ref. [27] and references therein)

$$y_{t1} = \frac{3(2g-1)}{2g}, \quad (9a)$$

$$y_{t2} = \frac{4(g-1)}{g}, \quad (9b)$$

and the corresponding magnetic exponents y_{h1} and y_{h2} are

$$y_{h1} = \frac{(2g+1)(2g+3)}{8g}, \quad (10a)$$

$$y_{h2} = \frac{(2g-1)(2g+5)}{8g}. \quad (10b)$$

The subleading thermal exponent (9b) corresponds to the so-called dilution operator. This one is relevant for the tricritical Potts model and irrelevant for the critical Potts model. At the critical 4-state Potts model, corresponding to $g = 1$, that operator is marginal with $y_{t2} = 0$. More precisely, the dilution operator is in this case marginally irrelevant; this is the origin of multiplicative [28, 29] and additive [30] logarithmic corrections.

There are also exponents that are linked to the geometric properties of the FK clusters, like their fractal dimension d_f [27], which is equal to the leading magnetic exponent y_{h1} (10a),

$$d_f = y_{h1} = \frac{(2g+1)(2g+3)}{8g}, \quad (11)$$

and the so-called hull exponent [31]

$$d_H = \frac{1+2g}{2g}. \quad (12)$$

Note that the above exponents, as well as many others, are rational functions of g ; but this is not true in general:

the backbone exponent for bond percolation d_B has been proven to be a transcendental number [32].

We expect that the FK clusters in the critical Potts model, at least for $Q \in [1, 4]$, and the clusters in the percolation model corresponding to $g = 2/3$ exhibit the same behavior of the size distribution n_s [c.f. Eq. (1)], with a Fisher exponent τ given by the hyper-scaling relation, and depending of g

$$\tau = 1 + \frac{d}{d_f} \stackrel{d=2}{=} \frac{3 + 24g + 4g^2}{(1 + 2g)(3 + 2g)}, \quad (13)$$

where $d = 2$ is the dimensionality of the lattice.

Our goal is to determine the correction-to-scaling exponent $\Omega(g)$ [c.f. Eq. (1)] of the size distribution of the FK clusters for both the critical and tricritical Potts models. In Sec. III we will show a theoretical argument leading to the conjecture

$$\Omega = \frac{1}{g d_f} = \frac{8}{(2g + 1)(2g + 3)}. \quad (14)$$

In a second step, we want to check this result by using MC simulations [33]. In this part, we will consider only integer values of Q . It is well known that MC algorithms suffer from critical slowing-down (CSD): roughly speaking, close to a critical point, the autocorrelation times diverges like ξ^z , where ξ is the correlation length, and z is the dynamic critical exponent [34]. The mere existence of CSD limits the accuracy of the MC results. For local algorithms, CSD is severe: $z \approx 2$. A more efficient algorithm is the Swendsen–Wang (SW) cluster algorithm [35] for the Q -state Potts ferromagnet with integer $Q \geq 2$. It radically reduces the value of z ; but it can not completely eliminate CSD whenever the specific heat diverges, due to the Li–Sokal bound [36]

$$z \gtrsim \frac{\alpha}{\nu} = 2y_{t1} - 2 = \frac{4g - 3}{g}. \quad (15)$$

Thus, we have $z > 0$ whenever $Q > 2$ ($g > 3/4$) for the Potts model. Other cluster [37, 38] and worm-type [39, 40] algorithms for the Potts model also satisfy some kind of Li–Sokal bound; therefore, CSD is always present.

In any MC study, one usually needs to extrapolate from a series of numerical measurements of a physical quantity $Q_c(L)$ (performed for simplicity at the critical temperature) on 2D systems of linear sizes $L \in \{L_1, L_2, \dots, L_k\}$, to the behavior of Q_c in the thermodynamic limit $L \rightarrow \infty$. This is achieved by performing fits to the *Ansatz*:

$$Q_c(L) = Q_{c,o} + L^{p_Q} [a_0 + a_1 L^{-\omega_1} + a_2 L^{-\omega_2} + \dots], \quad (16)$$

where $0 < \omega_1 < \omega_2 < \dots$, and the dots stand for higher-order corrections. It is clear that the larger the correction-to-scaling exponents ω_i , the more precise estimates of the three most-relevant parameters $\{Q_o, p_Q, a_0\}$ will be obtained. These correction-to-scaling exponents

not only come from the full set of subleading exponents [e.g., y_{t2} (9b) or y_{h2}]. They are also generated by the nonlinear relations between the standard thermodynamic parameters (e.g., temperature, magnetic field, etc) and the RG nonlinear scaling fields (see [41], and references therein). These “analytic” corrections provide integer correction-to-scaling exponents. In addition, we have a particular model which merits special attention. The critical 4-state Potts model has $y_{t2} = 0$, and this fact implies the existence of the aforementioned logarithmic corrections, which are very difficult to deal with.

Therefore, instead of simulating the original (3) or the diluted (6) Q -state Potts models to check conjecture (14), we will simulate yet another model. The $O(n)$ loop model on a finite 2D hexagonal lattice G [42–45] is given by the partition function

$$Z_{\text{loop}}(G; x, n) = \sum_{\{\ell\}} x^{E(\ell)} n^{N(\ell)}, \quad (17)$$

where the sum is over all possible non-intersecting loop configurations ℓ on G , $N(\ell)$ is the number of loops in the configuration, and $E(\ell)$ is the total length of all the loops. The parameter n represents the weight associated to each loop, and x is a fugacity that controls the weight of the loop’s length. We assume here that n, x are real positive parameters, so that (17) has a probabilistic interpretation.

We will see in Sec. II, that the free energy of the $O(n)$ loop model has been solved along two curves [42, 46, 47]

$$x_{\pm} = \frac{1}{\sqrt{2 \pm \sqrt{2 - n}}}. \quad (18)$$

These two curves are depicted in Fig.1. The curve $x_+(n)$ corresponds to the critical line of the $O(n)$ loop model separating the diluted phase from the dense phase. The RG analysis of this model shows that the RG trajectories corresponds to constant values of n . Therefore, for a fixed value of $n \in [0, 2]$, the interval $x \in (0, x_+(n))$ corresponds to the diluted phase, and $x \in (x_+(n), \infty)$, to the dense (or densely-packed) phase.

Furthermore, the critical $O(n)$ loop model has a CG representation [26, 27] with coupling strength g , where

$$n = -2 \cos(\pi g), \quad g \in [1, 2]. \quad (19)$$

Therefore, for a fixed value of $n \in [0, 2]$, the point $(1/x, n) = (1/x_+(n), n)$ belongs the same universality class as the tricritical Potts model with $Q = n^2$ states [cf. (8)/(19)].

The leading thermal exponent for this model is given by [42]

$$y_{t1}^{\text{loop}} = y_{t2} = \frac{4(g - 1)}{g}, \quad (20)$$

where y_{t2} is given by (9b). Thus, the leading thermal eigenvalue for the $O(n)$ model is the first subleading thermal exponent for the Potts model. The leading magnetic

exponent is given by [27, 42]

$$y_{h1}^{\text{loop}} = \frac{(2+g)(2+3g)}{8g}. \quad (21)$$

Note that this expression is equal to $y_{h1}(1/g)$ [cf. (10a)].

Given a fixed value of $n \in [0, 2]$, every point in the interval $1/x \in (0, 1/x_+(n))$ renormalizes towards a fixed point that belongs to the universality class of the critical Potts model with $Q = n^2$ states. In fact, x_- [cf., (18)] is the analytic extension of x_+ when $g \in [1/2, 1]$. Thus, formulas (20)/(21) are also valid when $g \in [1/2, 1]$.

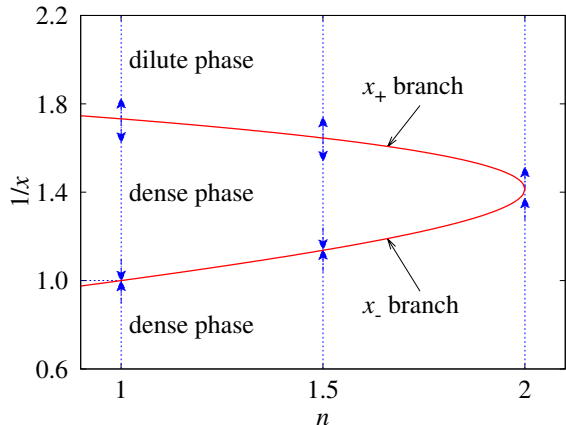


FIG. 1. Phase diagram of the $O(n)$ loop model on the hexagonal lattice for $n \in [1, 2]$. The system is in the dilute phase if the bond weight satisfies $x > x_+$, and in the dense phase if $x < x_+$. Vertical blue arrows sketch the directions of the RG flows. In terms of universality, the x_+ (resp. x_-) branch corresponds to the tricritical (resp. critical) Potts model.

Notice that on both curves x_{\pm} , the leading eigenvalue is the subleading eigenvalue y_{t2} of the Potts model; thus it is smaller than the Potts leading one y_{t1} . In addition, on $x_-(n)$, $y_{t2} < 0$; i.e., it is irrelevant. Therefore, the correction-to-scaling corrections are smaller than in the Potts model. Furthermore, the Li-Sokal bound becomes

$$z \gtrsim \frac{\alpha}{\nu} = 2y_{t1} - 2 = \frac{2(3g-4)}{g}. \quad (22)$$

This implies that $\alpha/\nu \leq -2$ on $x_-(n)$, and $\alpha/\nu \leq 0$ on $x_+(n)$ for $n \geq 1$. Thus, there is no obstacle for no CSD in this model. In this sense, highly efficient cluster algorithms for the $O(n)$ loop model with $n \geq 1$ have been proposed in the literature [48–51].

We may expect that the $O(n)$ loop model and the Potts model with $Q = n^2$ states that have the same CG coupling g do belong to the same universality class. The main assumption in this work is that the FK clusters of the critical and tricritical Potts models have the *same* critical behavior as the domains enclosed by the $O(n)$ loops. This hypothesis has been supported by analytic results for the fractal dimension d_f or the one associated to the breakdown of cubic symmetry d_{CM} [27]. In [51]

the backbone and shortest-path exponents for the $O(n)$ loop model are shown to coincide in both models. Notice that they also conclude the absence of multiplicative and additive logarithmic corrections for $Q = 4$. Therefore, performing the MC simulation on the $O(n)$ loop model has several advantages with respect to standard simulations on the Potts model.

The remainder of this paper is organized as follows. Section II describes in detail the $O(n)$ model and its critical behavior. In Sec. III, we show the theoretical argument leading to our conjecture for Ω [c.f. Eq. (14)]. Monte Carlo simulations and measurements are discussed in Sec. IV, and in Sec. IV, we present the numerical results. A brief discussion is given in Sec. V.

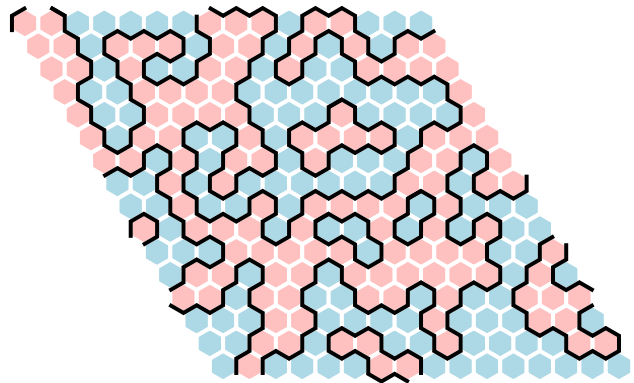


FIG. 2. Illustration of the correspondence between the $O(n)$ loop model on a hexagonal lattice with periodic boundary conditions and the generalized Ising model on the dual triangular lattice. The blue and red hexagons represent different Ising spins (up or down), while the black lines depict the domain walls between the generalized Ising spins, which correspond to the configurations of the $O(n)$ loop model.

II. THE $O(n)$ MODEL

Let us consider a graph G which is equal to a finite subset of the hexagonal lattice with some boundary conditions. A loop in G is a subgraph of G which is isomorphic to a cycle. A loop configuration ℓ is a spanning subgraph of G such as every vertex (or site) has even degree. Therefore, a loop configuration ℓ may contain isolated vertices. If we denote by $L(G)$ such a configuration space, the partition function of the $O(n)$ loop model [42–45] on G is given by

$$Z_{\text{loop}}(G; x, n) = \sum_{\ell \in L(G)} x^{E(\ell)} n^{N(\ell)} \quad (23)$$

[cf. (17)]. We start with real non-negative parameters x and n , so (23) has a probabilistic interpretation. As (23) is a polynomial jointly in x, n , we can promote these variables to arbitrary real or complex variables. An $O(n)$ loop configuration on a hexagonal lattice with periodic boundary conditions is depicted in Fig. 2

For $n = 0$, one recovers formally the self-avoiding random walk model. For $n = 1$, the $O(n)$ loop model is equivalent to the usual Ising model, and for $n = 2$, it corresponds to the XY model.

The $O(n)$ loop model has been solved by Nienhuis [26, 42] and Baxter [46, 47] on the curves (18). In particular, there is a phase transition at $x_c(n) = x_+(n)$:

$$x_c = x_+ = \frac{1}{\sqrt{2 + \sqrt{2 - n}}}, \quad -2 \leq n \leq 2. \quad (24)$$

In this paper, let us assume that $n \in [0, 2]$. The phase-transition line (24) separates a diluted phase from a dense phase. The diluted phase $x < x_c(n)$ is, roughly speaking, a disordered phase with exponential decay of correlations. If $x \geq x_c(n)$, the model should be critical, with algebraic decay of correlations. In this case, the model is governed in the thermodynamic limit by some CFT. Actually, there are two distinct critical regimes: $x = x_c(n)$ and $x > x_c(n)$, each of them with a distinct scaling limit. Figure 1 shows the phase diagram of the $O(n)$ loop model in the $(n, 1/x)$ plane. The two branches x_{\pm} (18) are shown, as well as the dilute and dense phases for $n \leq 2$. The phase diagram for $n > 2$ is beyond the scope of this paper.

Although the partition functions of the $O(n)$ loop model (17) and the Potts model (4)/(5) do not have a direct transformation, both can be represented in terms of a CG [27]. The RG analysis of the $O(n)$ loop model reveals that the RG trajectories correspond to constant values of n , and that, for each $n \in [0, 2]$, there are two types of fixed points (see Fig. 1) parametrized by (19). The $x_+ = x_c$ branch corresponds to $1 \leq g \leq 2$, and represents unstable fixed points, indicating a second-order phase transition from the dilute phase to the dense phase (or the tricritical point of the Potts model). The x_- branch (which is the analytic continuation of the former branch) corresponds to $1/2 \leq g < 1$, and represents stable fixed points, reflecting the universality of the whole critical dense phase (or the ordinary critical point of the Potts model). We can then unify formulas (8)/(19) as

$$\sqrt{Q} = n = -2 \cos(\pi g), \quad g \in \left[\frac{1}{2}, 2 \right]. \quad (25)$$

The physics of each of the points on x_c is given by a CFT of central charge [52]

$$c(g) = 1 - \frac{6(1-g)^2}{g}, \quad g \in [1, 2]. \quad (26)$$

This equation can be analytically continued to cover also the critical Potts model when $g \in [1/2, 1]$. Note that the conformal charge of the dense phase at $n = \sqrt{Q} = \sqrt{2}$ or $g = 3/4$ (the critical Ising model) is the same as the conformal charge at $x_c(1)$ or $g = 4/3$ (the one-state tricritical Potts model).

It is worth noticing that the critical value $x_c(0) = (2 + \sqrt{2})^{-1/2}$ has been rigorously obtained in Ref. [53]. On

the other hand, at the point $(n, x) = (2, 1/\sqrt{2})$, both branches x_{\pm} merge. This point corresponds to the critical 4-state Potts model.

As seen in the introduction, the leading thermal eigenvalue y_{t1}^{loop} (20) is not the leading thermal eigenvalue of the Potts model y_{t1} (9a), but the second leading eigenvalue y_{t2} (9b). As remarked in [48], the exponents y_{t1} and y_{h1} are *absent* in spin and loop observables in the $O(n)$ model; but they can be seen in observables associated to other objects, like faces. The $O(n)$ magnetic exponent (21) also appears in connection to an observable related to the worm MC algorithm [50].

Finally, at $x = \infty$ or $1/x = 0$, there is another phase in the $O(n)$ loop model dubbed the fully-packed phase. This phase is also critical, but its universality class is distinct from that of the dense phase [54–56]. The physical properties of this phase are beyond the scope of the present article.

III. THE CORRECTION-TO-SCALING EXPONENT Ω

In this section, we will derive the conjecture (14) for the correction-to-scaling exponent Ω [cf. Eq. (1)], thereby extending Ziff's result for percolation $\Omega = 72/91$ [4]. As in Ziff's paper, we will start from a formula due to Cardy [57] that gives the partition function of the $O(n)$ model on an annulus.

Let us consider the annulus $0 \leq x < \ell$ and $0 < y < L$ with periodic boundary conditions along the x -axis (i.e., we identify $x = 0$ and $x = \ell$), and free boundary conditions along the y -axis. In this section ℓ will denote the largest linear size of the annulus; we hope there is no confusion with the same letter denoting loop configurations in (17)/(23). We introduce the modulus

$$\tilde{q} = e^{-2\pi L/\ell}. \quad (27)$$

If we conformally map this region to an annulus of inner radius R_1 , and outer radius R , then $\tilde{q} = R_1/R$.

The partition function of the $O(n)$ model on this annulus is given by [57, formula on top of page 11]

$$Z(\chi') = \frac{Z_o}{\sin \chi'} \sum_{m \in \mathbb{Z}} a_m(\chi') \tilde{q}^{\frac{(\chi' + 2\pi m)^2 - \chi'^2}{2\pi^2 g}} \quad (28)$$

where

$$Z_o = \sqrt{\frac{2}{g}} \tilde{q}^{-\frac{c}{24}} \prod_{r=1}^{\infty} (1 - \tilde{q}^{2r})^{-1}, \quad (29a)$$

$$a_m(\chi') = \sin\left(\frac{\chi' + 2\pi m}{g}\right) \quad (29b)$$

Formulas (28)/(29) correspond to a $O(n)$ model with CG coupling g , conformal charge $c = c(g)$ given by (26), and

angle χ . This angle is related to g by the standard formula

$$\chi = \pi(1 - g), \quad (30)$$

and to the loop weight by $n = \sqrt{Q} = 2 \cos \chi$. Again $g \in [1, 2]$ corresponds to the tricritical Q -state Potts model, and $g \in [1/2, 1]$, to the critical Q -state Potts model. The other angle χ' corresponds to the weight given to the loops that wrap non-trivially around the annulus $n' = 2 \cos \chi'$. Note that Z_o (29a) is independent of χ' .

We now extract the terms independent of m in the sum of Eq. (28):

$$Z(\chi') = \frac{Z_o}{\sin \chi'} \tilde{q}^{\frac{\chi'^2 - \chi^2}{2\pi^2 g}} \sum_{m \in \mathbb{Z}} a_m(\chi') \tilde{q}^{\frac{2(\pi m^2 + \chi' m)}{\pi g}}. \quad (31)$$

If we set $\cos \chi' = 0$ (i.e., $\chi' = \pi/2$), we suppress all contributions with a nonzero number of loops wrapping around the annulus. This happens if and only if there is a cluster connecting both boundaries at $y = 0$ and $y = L$. Therefore, the leading term of the crossing probability $\Pi(\tilde{q})$ that there is a cluster connecting the boundaries is given in the limit $\tilde{q} \rightarrow 0$ or $R_1/R \rightarrow 0$ by

$$\begin{aligned} \Pi(\tilde{q}) &= \frac{Z(\pi/2)}{Z(\chi)} \sim \tilde{q}^{1/(8g) - (1-g)^2/(2g)} \\ &= \left(\frac{R_1}{R}\right)^{1-g/2-3/(8g)}. \end{aligned} \quad (32)$$

The contributions from the sum in (31) when $\chi' = \pi/2$ is given by

$$\begin{aligned} \sum_{m \in \mathbb{Z}} a_m(\pi/2) \tilde{q}^{\frac{2(\pi m^2 + \pi m/2)}{\pi g}} &= a_0 + a_{-1} \tilde{q}^{1/g} \\ &+ a_1 \tilde{q}^{3/g} + \dots \end{aligned} \quad (33)$$

The contribution of the sum when $\chi' = \chi$ [cf. (30)] is

$$\begin{aligned} \sum_{m \in \mathbb{Z}} a_m(\chi) \tilde{q}^{\frac{2(\pi m^2 + \chi m)}{\pi g}} &= a_0 + a_{-1} \tilde{q}^2 \\ &+ a_1 \tilde{q}^{4/g-2} + \dots \end{aligned} \quad (34)$$

As $g \in [1/2, 2]$, both series generically have a nonzero leading term, and the most relevant correction term is $\tilde{q}^{1/g}$ from (33).

Therefore, the leading term of the crossing probability (32) is given by

$$\begin{aligned} \Pi\left(\frac{R}{R_1}\right) &\sim \left(\frac{R}{R_1}\right)^{g/2+3/(8g)-1} [1 + A \tilde{q}^{1/g} + \dots] \\ &= \left(\frac{R}{R_1}\right)^{d_f-2} \left[1 + A \left(\frac{R}{R_1}\right)^{-1/g} + \dots\right] \end{aligned} \quad (35)$$

where d_f is the fractal dimension (11).

Now we argue in the same way as in Ref. [4]. The probability $\Pi(R/R_1)$ can be related to the probability at criticality $P_{\geq s}$ that an occupied vertex is connected to a cluster of size greater than or equal to s . This latter probability is given by

$$P_{\geq s} \sim s^{2-\tau} (1 + A s^{-\Omega} + \dots), \quad (36)$$

where τ is the Fisher exponent. At the critical temperature, the clusters are fractal objects, so their size s and their radius R are related as

$$s \sim \left(\frac{R}{\epsilon}\right)^{d_f}, \quad (37)$$

where ϵ is some length of the order of the lattice spacing, and d_f is the fractal dimension (11). If we assume that $\epsilon = R_1$, we have that the probability of having a cluster of radius equal to or greater than R is given by

$$P_{\geq R} \sim R^{(2-\tau)d_f} (1 + A' R^{-\Omega d_f} + \dots). \quad (38)$$

Indeed, if we introduce the hyperscaling relation for τ (13), we have that

$$(2 - \tau) d_f = \left(1 - \frac{2}{d_f}\right) d_f = d_f - 2, \quad (39)$$

which is the leading exponent in (35). Therefore, the first correction-to-scaling exponent should satisfy

$$\frac{1}{g} = \Omega d_f, \quad (40)$$

which is the conjecture (14).

Note that the difference between the two most relevant magnetic eigenvalues [cf. Eq. (10)] is precisely the leading correction-to-scaling term in (35)

$$y_{h2} - y_{h1} = -\frac{1}{g}. \quad (41)$$

In other words, the fractal structure of the critical FK clusters should be characterized by both the leading and subleading magnetic exponents (10). If R_s is the radius of a cluster of size s , one expects

$$s \sim R_s^{y_{h1}} (1 + b R_s^{y_{h2} - y_{h1}} + \dots). \quad (42)$$

IV. MONTE CARLO ALGORITHM

In this section, we will discuss in more detail the MC algorithm used in the simulations of the $O(n)$ model on the hexagonal lattice performed in this work to check conjecture (14).

There are several MC algorithms that can be used to efficiently simulate the $O(n)$ loop model on the hexagonal lattice: the worm algorithm [50], and extensions of the cluster Chayes–Machta [37] algorithm; see e.g., [48, 51].

Let us assume in this section that the graph G is planar; e.g., a finite subset of the hexagonal lattice with free boundary conditions. We also consider integer values of $Q = n^2$.

In the actual MC simulations, we will employ the efficient cluster algorithm developed in Refs. [51, 58], which is based on the so-called induced-subgraph picture and was originally introduced by Chayes and Machta [37].

Basically, we start from the partition function of the model (17), and split the weight n as follows:

$$n = n_\alpha + n_\beta = 1 + n_\beta, \quad (43)$$

where α (resp. β) stands for the ‘‘active’’ (resp. ‘‘inactive’’) color in the Chayes–Machta language. Now, given a loop configuration of the hexagonal lattice, we assign, independently for each loop, the active color α with probability $1/n$, or the inactive color β with probability $1 - 1/n$. So all vertices in a given loop have the same color. In addition, we assign the active color α to all vertices that do not belong to any loop. This is consistent with the fact that these vertices have an implicit weight equal to one in (17). We have obtained an induced $O(1)$ (i.e., Ising) model on the active vertices. This induced model can be simulated by any valid MC algorithm.

It is important to realize that the loops in an $O(n)$ configuration on the hexagonal lattice can be regarded as domain boundaries of an Ising model of the dual triangular lattice; i.e., they represent the borders between spin-up and spin-down regions. This correspondence allows us to map the loop model on the hexagonal lattice G to a generalized Ising model on the dual triangular lattice G^* . Note that this statement is true due to the planarity of G . Due to the spin-flip symmetry in the Ising model, there is actually a one-to-two correspondence between loop configurations and dual Ising spin configurations. If K^* is the nearest-neighbor coupling for the dual Ising model [59], the bond weight x is given by

$$2K^* = -\log(x). \quad (44)$$

Indeed, when $0 < x < 1$, the Ising model is ferromagnetic (for $x > 1$, the system is antiferromagnetic). The partition function of this generalized Ising model on the dual triangular lattice $G^* = (V^*, E^*)$ is given by

$$Z_{\text{GIsing}}(G^*; K^*, n) = \sum_{\{s\}} n^{\mathcal{N}_d} \prod_{\{i,j\} \in E^*} e^{K^* s_i s_j}, \quad (45)$$

where $\mathcal{N}_d = \mathcal{N}_\ell + 1$ is the number of spin domains (within each spin domain, spins are identical), and the summation is over all Ising configurations. The relation between the $O(n)$ model on the hexagonal lattice and the generalized Ising model (45) on the dual triangular lattice is shown in Fig. 2. The $O(n)$ loops live on the edges of the original hexagonal lattice, while the Ising spins live on the vertices of the dual triangular lattice. The value of these Ising spins is given by the color of the corresponding face.

We can now apply the induced subgraph method to the generalized Ising model (45) on G^* . From any given spin configuration, we compute the corresponding spin domains. Then, independently for each spin domain, we assign the active color α (resp. inactive color β) with probability $1/n$ (resp. $1 - 1/n$). In this way, we obtain a random partition of the lattice $G^* = (V^*, E^*)$. The vertex set is naturally split as $V^* = V_\alpha^* \cup V_\beta^*$. The edge set is also partitioned into $E^* = E_\alpha^* \cup E_\beta^* \cup E_{\alpha\beta}^*$. Here, E_a^* (with $a = \alpha, \beta$) is the subset of edges whose endpoints both belong to V_a^* . The set $E_{\alpha\beta}^*$ contains all edges such that one vertex belongs to V_α^* , and the other to V_β^* .

Note that we have an induced Ising model on the active subgraph G_α^* ; this model can be simulated using the SW algorithm [35]. The probability p that a bond is occupied is chosen, when the system is ferromagnetic ($0 < x < 1$), as $p = 1 - e^{-2K^*} = 1 - x$ for each pair of parallel neighboring spins. If the system is antiferromagnetic ($x > 1$), the bond occupation probability is $p = 1 - e^{2K^*} = 1 - 1/x$ for each pair of anti-parallel neighboring spins. This step needs some extra care: all edges not belonging to E_α^* must be occupied to ensure that the domain topology of the inactive subgraph $G^* \setminus G_\alpha^*$ remains unchanged.

In practice, we are going to simulate the generalized Ising model (45) on finite triangular lattices of size $L \times L$ with periodic boundary conditions. This model is not, strictly speaking, identical to the $O(n)$ loop model on a finite hexagonal lattice with periodic boundary conditions. Nevertheless, such a boundary difference is expected to play a negligible role in the bulk critical phenomena, and indeed, no practical effect has been observed in previous studies [51].

The detailed procedure is as follows:

- (1) Independently for each spin domain, choose the active color α with probability $1/n$, or the inactive color β with probability $1 - 1/n$.
- (2) Independently for each edge $e \in E^*$, place an occupied bond with probability p . For the ferromagnetic case $x \in (0, 1)$, this probability is given by

$$p = \begin{cases} 1 - x & \text{if } s_i = s_j, \text{ and } e \in E_\alpha^*, \\ 0 & \text{if } s_i \neq s_j, \text{ and } e \in E_\alpha^*, \\ 1 & \text{otherwise.} \end{cases} \quad (46)$$

For the antiferromagnetic case $x > 1$, we have

$$p = \begin{cases} 1 - \frac{1}{x} & \text{if } s_i \neq s_j, \text{ and } e \in E_\alpha^*, \\ 0 & \text{if } s_i = s_j, \text{ and } e \in E_\alpha^*, \\ 1 & \text{otherwise.} \end{cases} \quad (47)$$

- (3) We now obtain a cluster configuration on G_α^* . Note that, even for the ferromagnetic case, a cluster typically contains both $+1$ and -1 Ising spins. Independently, for each connected component, flip the Ising spins or keep the current Ising spins with probability $1/2$. The new loop configuration is the Peierls contour for the new Ising configuration.

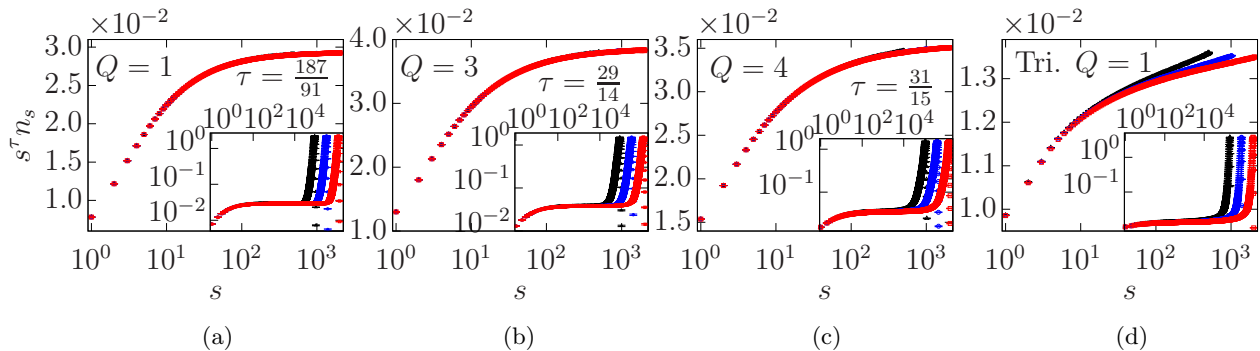


FIG. 3. Finite-cluster-size effects on n_s for the critical and tricritical Potts models. We plot the modified size distribution $s^\tau n_s$ of FK clusters versus s (with τ fixed at its exact value), in the critical $Q = 1$ (a), $Q = 3$ (b), and $Q = 4$ (c) Potts models, as well as in the tricritical $Q = 1$ (d) Potts model. The black, blue, and red data points correspond to systems of linear sizes $L = 512, 1024$ and 2048 , respectively. In the main figure of each panel, we have only displayed data with $s \leq L$, which has no wrapping effect. The excellent data collapse for the various system sizes in panels (a)–(c) shows that $n(s)$ on the x_- branch has no noticeable finite-lattice-size corrections. On the other hand, the main figure in panel (d) shows sizeable finite-lattice-size corrections. The Fisher exponent for the tricritical one-state Potts model (d) is $\tau = 379/187$. In each panel, the inset plots $s^\tau n_s$ for all values of s , demonstrating that the wrapping effect from periodic boundary conditions always exists.

It is known [51] that the above algorithm for the $O(n)$ loop model in the dense phase has no CSD. Along the dilute critical branch, the CSD is also completely absent for $1 < n < 2$; for $n = 1$, the algorithm just reduces to the standard SW cluster method, which is known to have some minor CSD $z \approx 0.22$ [41]. In addition, since in this project we are interested in the geometric structure of the Ising domains, simulating the generalized Ising model (45) is also very convenient, as we do not have to go back and forth between the hexagonal and the triangular lattices.

V. RESULTS

We have simulated the generalized Ising model (45) on triangular lattices of size $L \times L$ with $L = 16, 32, \dots, 2048$, and periodic boundary conditions. We have selected the values $n = 1, \sqrt{2}, \sqrt{3}$ (i.e., $Q = 1, 2, 3$) along the x_- branch (18-), and $n = 1, \sqrt{2}$ along the x_+ branch (18+), as well as $n = 2$ (i.e., $Q = 4$) where x_\pm meet. For each system, we have generated over 10^6 statistically independent samples.

Studies on correction-to-scaling exponents in the percolation model, both numerical and theoretical, are typically conducted in infinite systems. In finite systems of linear size L , the critical divergent correlation length ξ is smeared out to be of order $O(L)$, and the size of the largest cluster scales as $\sim L^{d_f}$. As a result, the asymptotic cluster-size distribution $n_s \sim s^{-\tau}$ is modified to have a finite-lattice-size scaling form as

$$n_s \sim s^{-\tau} \tilde{n}(sL^{-d_f}), \quad (48)$$

where $\tilde{n}(x)$ is a universal function and, typically, decays exponentially for $x \gg 1$. To study the cluster-size distribution and particularly the finite-cluster-size corrections,

one should restrict to the region $1 \ll s \ll L^{d_f}$. In particular, to avoid any wrapping effects from the periodic boundary conditions, it would be even better to explore in the more restricted region $1 \ll s \leq L$.

Figure 3 illustrates the impact of finite-lattice-size effects and boundary conditions on the observable n_s by plotting $s^\tau n_s$ versus s for points on the two branches x_\pm (18). Panels (a) and (b) represent data on the x_- branch: (a) $n = 1$, and (b) $n = \sqrt{3}$, respectively. The main figure in these panels shows MC data for $L = 512, 1024$, and 2048 up to $s = L$; i.e., the linear size L is used as an upper cutoff. Moreover, the corresponding insets show the full data set. It can be observed in the insets that data points for $s \gtrsim L$ are clearly affected by finite-lattice-size effects. That is why we have used the system linear size L as an upper cutoff in our analysis. As discussed in the Introduction, RG studies indicate that for the $O(n)$ loop model on the x_- branch with $1 \leq n \leq 2$, the sub-leading eigenvalue y_{t2} becomes irrelevant. Therefore, its contribution to finite-lattice-size effects is negligible for all practical purposes. In panels (a) and (b), it is clear that the data for different system sizes fall on the same curve when L is used as a cutoff, indicating no system-size dependence. We can safely assume that we are working in the thermodynamic limit. Similar observations apply to panel (c), which corresponds to $n = 2$. At this point both branches x_\pm meet. However, we can see small finite-lattice-size effects for the $L = 512$ data. Finally, the rightmost panel (d) displays the data for $n = 1$ on the branch x_+ . In the main figure, we can observe a noticeable separation of the data points for $s \gtrsim 10^2$. This is a sign of significant finite-lattice-size effects, which make harder the data analysis for this branch.

A. Critical Potts model with $Q = 1, 2, 3$

In this section we will consider three points on the branch x_- , namely $Q = 1, 2, 3$ (or, equivalently, $n = 1, \sqrt{2}, \sqrt{3}$). These points belong to the universality class of the critical Q -state Potts model.

The size distribution of FK clusters at the critical point follows the behavior $n_s = s^{-\tau} (A + B s^{-\Omega} + \dots)$ for large enough values of s [cf. (1)]. The parameter τ is the Fisher exponent (13). We have employed a least-squares fit to the data using the transformed variable

$$s^\tau n_s = a + b_1 s^{-y_1}, \quad (49)$$

and performed a systematic analysis by applying different lower cutoffs $s \geq s_{\min}$. For fitting the data on the x_- branch, we have only used data from the largest system $L = 2048$, as the data for the smaller system sizes coincide perfectly for $s \geq 128$. We have also attempted to include an additional correction term $b_2 s^{-y_2}$ (with $y_2 > y_1 > 0$) in the Ansatz (49), but this did not result in smaller error bars for the final estimates. In Table I, we have summarized the results of the fits. For each value of $Q = 1, 2, 3$, we show several fits corresponding to distinct choices of the lower cutoff s_{\min} . For each fit, we display the parameters a, b_1 , and y_1 [cf. (49)], as well as the χ^2 and the number of degrees of freedom (DF) of the corresponding fit. When the cutoff s_{\min} is too small, finite-size effects at small s cause a significant increase in χ^2/DF .

The point $n = 1$ on the x_- branch corresponds to $g = 2/3$ and $\tau = 187/91 \approx 2.054945$. This is the bond-percolation critical point, for which the correction-to-scaling exponent has been precisely determined as $\Omega = 72/91 \approx 0.791209$ [4]. This value is also predicted by conjecture (14). We see in Table I that the results for $s_{\min} = 64, 128$ are compatible within errors, giving $\Omega = 0.795(5)$, which fully agrees with the above value. In Fig. 4(a), we display the data for $s^\tau n_s$ vs. $s^{-\Omega}$ with $\Omega = 72/91$. The agreement is very good for large enough values of s . In the inset, we show the full data set, and we see that at small values of s , the behavior of $s^\tau n_s$ vs. $s^{-\Omega}$ is no longer linear, as expected. In this regime, additional correction-to-scaling terms should contribute, and the simple Ansatz (49) is not valid any more.

The point $n = \sqrt{2}$ on the x_- branch corresponds to $g = 3/4$ and $\tau = 31/15 \approx 2.066667$. This is the critical point of the Ising model. Conjecture (14) predicts $\Omega = 32/45 \approx 0.711111$. We see in Table I that the results for $s_{\min} = 64, 128$ are compatible within errors, giving $\Omega = 0.723(6)$, which agrees within two standard deviations from the conjectured value. In Fig. 4(b), we display the data for $s^\tau n_s$ vs. $s^{-\Omega}$ with $\Omega = 32/45$. Again the agreement for large s is very good; while at small values of s , we need more terms in the Ansatz (49).

The point $n = \sqrt{3}$ on the x_- branch corresponds to $g = 5/6$ and $\tau = 29/14 \approx 2.071429$. This is the critical point of the 3-state Potts model. Conjecture (14)

TABLE I. Power-law fits (49) to the Monte Carlo data for the critical Potts model with $Q = 1, 2, 3$ states. For each value of Q , we provide two distinct fits, each of them corresponding to a different lower cutoff $s \geq s_{\min}$ with $s_{\min} = 64, 96, 128$. For each single fit, we provide the estimates of the free parameters a, b_1, y_1 , as well as the values of the χ^2 and the number of degrees of freedom (DF) of the fit. The entries with an exact number for y_1 correspond to the two-parameter fits to the Ansatz (49) where y_1 is fixed to the conjectured value for Ω (14).

Q	s_{\min}	y_1	b_1	a	χ^2/DF
1	64	0.790(2)	-0.0461(3)	0.029351(2)	328.6/317
	96	0.796(3)	-0.0472(6)	0.029347(2)	281.4/285
	128	0.795(5)	-0.047(1)	0.029347(3)	251.7/253
	96	72/91	-0.04639(4)	0.0293501(8)	283.4/286
	128	72/91	-0.04633(6)	0.0293495(9)	252.3/254
160	72/91	-0.04621(9)	0.029348(1)	237.7/238	
2	64	0.716(2)	-0.0480(3)	0.036014(3)	336.9/317
	96	0.723(4)	-0.0494(7)	0.036006(5)	307.1/285
	128	0.723(6)	-0.049(1)	0.036006(6)	267.3/253
	96	32/45	-0.04714(5)	0.036021(1)	318.2/286
	128	32/45	-0.04699(8)	0.036018(2)	272.1/254
160	32/45	-0.0469(1)	0.036016(2)	246.2/238	
3	64	0.647(2)	-0.0430(3)	0.038649(5)	324.7/317
	96	0.647(4)	-0.0430(6)	0.038649(7)	303.4/285
	128	0.639(6)	-0.0415(10)	0.038660(9)	267.9/253
	96	9/14	-0.04228(5)	0.038657(2)	304.8/286
	128	9/14	-0.04215(7)	0.038654(2)	268.4/254
160	9/14	-0.0421(1)	0.038654(3)	257.7/238	

predicts $\Omega = 9/14 \approx 0.642857$. We see in Table I that the results for $s_{\min} = 64, 96$ are compatible within errors, and they differ by two standard deviations from the results with $s_{\min} = 128$. This differences can be explained by systematic errors not taken into account in the Ansatz (49). Our preferred estimate would be the one for $s_{\min} = 128$ with some conservative error bars to take into account the behavior of the estimates versus s_{\min} : $\Omega = 0.638(9)$. The agreement with the conjectured value is very good. In Fig. 4(c), we display the data for $s^\tau n_s$ vs. $s^{-\Omega}$ with $\Omega = 9/14$. The same comments made for the other two values of Q apply in this case, too.

Ziff proposed an intuitive method to observe the value of Ω in the percolation model [4], which we have extended to the Potts model. The idea was to measure the probability $P_{\geq s}$ that an occupied site belongs to an FK cluster of size greater than or equal to s . Its behavior is similar to that in the percolation model

$$P_{\geq s} = s^{2-\tau} (A + B s^{-\Omega} + \dots). \quad (50)$$

The value of Ω can be directly assessed through

$$\bar{\Omega}(s) = -\log_2 \left(\frac{C_s - C_{s/2}}{C_{s/2} - C_{s/4}} \right) \quad (51)$$

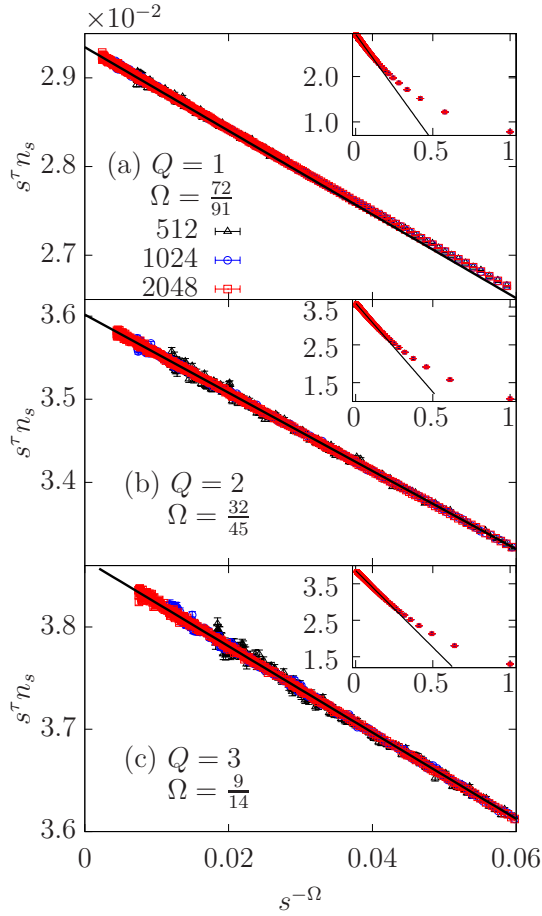


FIG. 4. Estimates of the correction-to-scaling exponent Ω for the critical Potts model with $Q = 1$ (a), $Q = 2$ (b), and $Q = 3$ (c). Each main figure depicts $s^\tau n(s)$ versus $s^{-\Omega}$ for various system sizes $L = 512$ (black), $L = 1024$ (blue), and $L = 2048$ (red). In these plots, Ω is fixed to its conjectured value (14), which is depicted in each panel. In each main plot we show the data with $s \gtrsim 35$. The black lines correspond to the two-parameter fit to the Ansatz (49) with Ω fixed to its conjectured value. In the insets, we show the full data set to highlight that, at small values of s , the behavior is not linear.

where

$$C_s = s^{\tau-2} P_{\geq s}. \quad (52)$$

The leading order of the linear combination $C_s - C_{s/2}$ equals $B(1 - 2^\Omega) s^{-\Omega}$; this implies formula (51). Due to higher-order correction-to-scaling effects, $\bar{\Omega}$ deviates from Ω at small s , but gradually approaches to Ω as s increases.

Figure 5 shows the plots $\bar{\Omega}$ vs. s for the critical Potts model with $Q = 1$ (a), 2 (b), and 3 (c). The vertical dashed line represents $s = 2048$, corresponding to the upper cutoff to the data point with $L = 2048$ (red points). It can be observed that the error bars significantly increase when $s \geq L$, consistent with the previous truncation of n_s data. We have fitted the data to a power-law

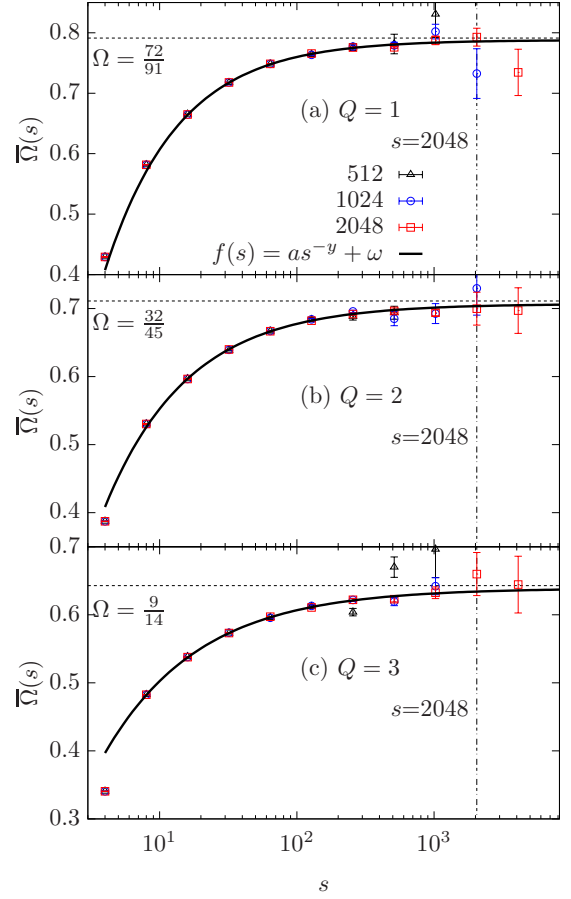


FIG. 5. Quantity $\bar{\Omega}$ (51) for the critical Potts model. We show the plots of $\bar{\Omega}(s)$ vs. s to show our conjectured correction-to-scaling exponent Ω for the critical Potts model with $Q = 1$ (a), 2 (b), and 3 (c). Each figure plots $\bar{\Omega}(s)$ for three various system sizes $L = 512, 1024, 2048$ by choosing $s = 4, 8, \dots, 2L$. The vertical dashed line indicate $s = 2048$, which is the linear system size for $L = 2048$ data points. Note that for $s > L$, the error bars for the data are significantly larger compared to those with $s \leq L$. The horizontal dashed lines represent our conjectured correction-to-scaling exponent Ω (14). The black curves represent fits to the $L = 2048$ data (red points) to the Ansatz (53), excluding the $s \geq L$ data points.

Ansatz

$$\bar{\Omega}(s) = \omega + a s^{-y}, \quad y > 0. \quad (53)$$

The second term in this Ansatz takes into account higher-order corrections. We have included in the fits the data for $\bar{\Omega}$ with $s < s_{\max} = L$. The horizontal dashed lines in Figure 5 indicate the conjectured values for Ω , and the gradual approach of $\bar{\Omega}$ to the conjectured value of Ω as s increases further supports our Ansatz (53).

The critical hexagonal-lattice $O(1)$ loop model in the dense phase is equivalent to site percolation on the dual triangular lattice. Ziff has already studied the properties of this latter system in the thermodynamic limit [4].

We have plotted $\bar{\Omega}$ versus s for various system sizes in Fig. 5(a). The behavior is consistent with Ziff's results. We then fitted the $\bar{\Omega}$ data to the Ansatz (53), excluding the points with $s \geq L$ to eliminate the effects of wrapping clusters. The estimates from the fit yielded $a = -1.17(4)$, $y = 0.81(2)$, and $\omega = 0.788(2)$. This result differs by 1.6 standard deviations from the exact result $\Omega = 72/91$.

To deal with the critical Potts model with $Q = 2$ and $Q = 3$, we have used a similar method to fit the data for $s \leq L$. The results for $Q = 2$ of the fits to the Ansatz (53) are $a = -0.81(2)$, $y = 0.72(1)$, and $\omega = 0.707(3)$. This estimate differs from the exact value $\Omega = 32/45$ in 1.4 standard deviations [see Figure 5(b)]. For $Q = 3$, we have $a = -0.57(2)$, $y = 0.62(2)$, and $\omega = 0.639(3)$. In this case, the latter estimate is 1.3 standard deviations away from the exact value $\Omega = 9/14$ [see Figure 5(c)]. It can be seen in Figs. 5(b)–(c) that the data points approach the expected value in a similar way as in Fig. 5(a).

B. Tricritical Potts model with $Q = 1, 2, 3$ and $Q = 4$

In this section we will consider two points on the branch x_+ , namely $Q = 1, 2$ (or, equivalently, $n = 1, \sqrt{2}$). These points belong to the universality class of the tricritical Q -state Potts model. In addition, we will consider the critical Potts with $Q = 4$ states (or, equivalently, $n = 2$). At this point, both branches x_{\pm} merge, and sophisticated finite-lattice-size corrections might occur. Note that the case $Q = 3$ has not been studied, as the results should behave in a similar way as those for $Q = 2, 4$.

The tricritical Potts model corresponds to the unstable fixed point of the $O(n)$ loop model. We have assumed that the size distribution n_s of the FK clusters exhibits the same behavior as in the critical Potts model (1), and that our conjectured formula for the correction-to-scaling exponent is given by formula (14). In contrast to the dense branch x_- , the subleading thermal scaling field is relevant ($y_{t2} > 0$) along the dilute branch x_+ . As a consequence, the thermal fluctuations become significant, contributing as a source of finite-lattice-size corrections, and becoming more and more severe as n decreases (i.e., as we approach $n = Q = 1$).

The above argument implies, in practice, that a direct fit of the n_s data to the Ansatz (49) does not yield stable results. If we plot $s^{\tau} n_s$ vs. $s^{-\Omega}$ using the conjectured value for Ω (14), we obtain Fig. 6. In the insets of the panels, we observe that the behavior is not linear when s is small (as in Sec. VA), but also for large enough values of s , as it can be seen in the main panels of Fig. 6. In this figure, we have depicted data for three values of $L = 512, 1024$, and 2048 . This latter effect is due to strong finite-size-scaling corrections. Indeed, as L grows, the behavior of the corresponding data becomes linear in a wider interval of s . In order to isolate the linear regime of $s^{\tau} n_s$ vs. $s^{-\Omega}$, we have considered, for each value

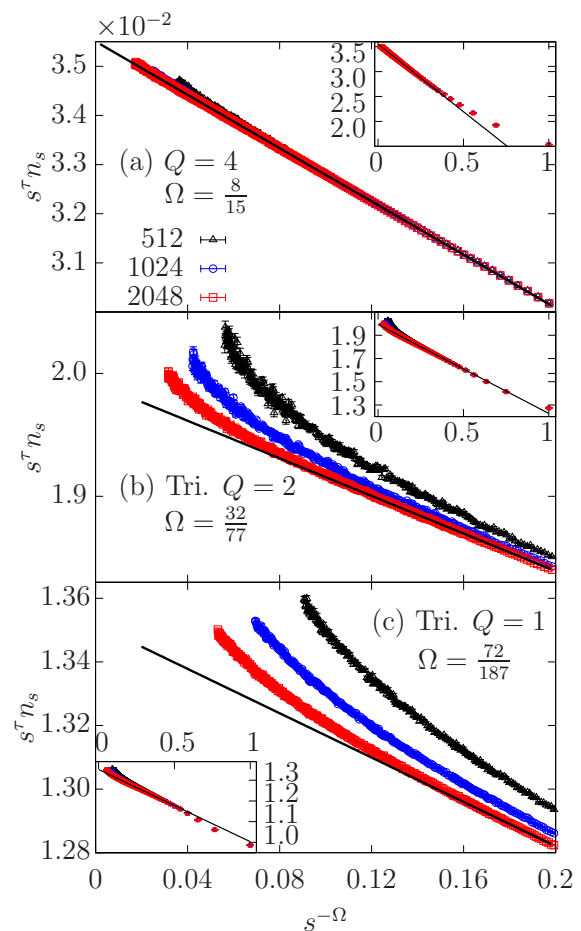


FIG. 6. Estimates of the correction-to-scaling exponent Ω for the critical Potts model with $Q = 4$ (a) and for the tricritical Potts model with $Q = 2$ (b), and $Q = 1$ (c). Each main figure depicts $s^{\tau} n(s)$ versus $s^{-\Omega}$ for various system sizes $L = 512$ (black), $L = 1024$ (blue), and $L = 2048$ (red). In these plots, Ω is fixed to its conjectured value (14), which is depicted in each panel. The black lines correspond to the two-parameter fit to the Ansatz (49) with Ω fixed to its conjectured value. In each main plot we show the data with $s \gtrsim 21$. In the insets, we show the full data set to highlight the effects at large and small values of s .

of L , the data in the interval $[s_{\min}, s_{\max}]$ for some values of $s_{\min} < s_{\max}$. Then, by varying systematically both s_{\max} and s_{\min} , we have been able to fit the data to the Ansatz (49), and in this case we have obtained stable results for the three values of L we have considered in this analysis. The solid lines in Fig. 6 represent the best fit for the largest-size data ($L = 2048$). In Table II, we have summarized the results of the fits. For each value of $Q = 4, 2, 1$, we show several fits corresponding to distinct choices of the lower and upper cutoffs s_{\min}, s_{\max} . For each fit, we display the parameters a, b_1 , and y_1 [cf. (49)], as well as the χ^2 and the number of degrees of freedom (DF) of the corresponding fit.

The four-state critical Potts model ($g = 1$) has $\tau =$

TABLE II. Power-law fits (49) to the Monte Carlo data for the critical Potts model with $Q = 4$ states, and the tricritical Potts model with $Q = 1, 2$ states. For each value of Q , we provide several distinct fits, each of them corresponding to a different lower and upper cutoffs $s_{\max} \geq s \geq s_{\min}$. For each single fit, we provide the estimates of the free parameters a, b_1, y_1 , as well as the values of the residual χ^2 and the number of degrees of freedom (DF) of the fit. The entries with an exact number for y_1 correspond to the two-parameter fits to the Ansatz (49) where y_1 is fixed to the conjectured value for Ω (14).

Q	s_{\min}	s_{\max}	y_1	$b_1 \times 10^2$	$a \times 10^2$	χ^2/DF
4	32	512	0.5319(7)	-2.702(5)	3.5511(3)	259.7/221
	64	512	0.536(2)	-2.73(2)	3.5496(8)	212.8/189
	32	640	0.5315(7)	-2.700(5)	3.5513(3)	275.0/237
	64	640	0.534(2)	-2.72(2)	3.5505(6)	231.5/205
	32	768	0.5313(6)	-2.698(4)	3.5514(3)	290.0/253
	64	768	0.532(2)	-2.71(1)	3.5510(6)	248.3/221
	32	640	8/15	-2.7118(6)	3.55045(7)	283.5/238
	64	640	8/15	-2.714(1)	3.5506(1)	231.6/206
	96	640	8/15	-2.716(2)	3.5507(2)	191.5/174
	Tri. 2	16	96	0.419(2)	-0.767(2)	1.9907(8)
32		96	0.415(8)	-0.764(9)	1.992(3)	48.2/62
16		112	0.417(2)	-0.766(1)	1.9917(7)	91.2/94
32		112	0.409(6)	-0.758(7)	1.995(2)	65.9/78
16		128	0.416(1)	-0.765(1)	1.9921(6)	106.4/109
32		128	0.407(5)	-0.756(6)	1.995(2)	79.0/93
16		112	32/77	-0.7649(3)	1.99210(8)	91.6/95
32		112	32/77	-0.7655(8)	1.9922(2)	66.9/79
48		112	32/77	-0.767(2)	1.9924(3)	53.3/63
Tri. 1		24	68	0.372(4)	-0.344(1)	1.355(1)
	32	68	0.37(1)	-0.345(4)	1.355(2)	31.4/34
	24	68	72/187	-0.3486(2)	1.35174(6)	50.8/43
	32	68	72/187	-0.3494(4)	1.35193(8)	32.8/35

31/15 and we conjecture $\Omega = 8/15 \approx 0.533333$. The data presented in Fig. 6(a) shows a good agreement with a straight line in the region where $s \gg 1$. We also observe slight deviations from linearity for $s \gtrsim L$. We have performed a systematic fit of the data to the power-law Ansatz (49) by setting different upper and lower cutoffs s_{\min} and s_{\max} . First, we have selected the value of $s_{\max} \gtrsim L$ from Fig. 6(a) where no significant deviation from linearity is observed. We have then progressively chosen different values of s_{\min} in increasing order, and starting from $s_{\min} = 16$. If the variance of the residuals decreases when we increase s_{\min} , and the estimates for the parameters y_1 , a , and b_1 are stable within errors, then s_{\max} is considered a reasonable choice. Subsequently, s_{\max} is reduced, and the procedure is repeated to ensure the reliability of the fit. Some of the results are shown in Table II, where the fit is relatively stable for $s \leq 768$, yielding $\Omega = 0.534(4)$, which agrees very well with the conjecture.

The 2-state tricritical Potts model has $g = 5/4$, $\tau = 157/77$, and we conjecture $\Omega = 33/77 \approx 0.428571$. Following the same procedure as for $Q = 4$, we first plotted

$s^\tau n_s$ versus s in Fig. 6(b) using the conjectured value for Ω . As discussed earlier, if we are on the branch x_+ and the parameter n is decreased, the finite-size effects from L become larger. Although the data for different sizes exhibit a significant bifurcation as s approaches L , a clear linear behavior is observed in the intermediate region where s satisfies $L \gg s \gg 1$. We have performed fits to the Ansatz (49) by systematically applying different upper cutoffs for s . For $s \leq 128$, the results are relatively stable, yielding $\Omega = 0.41(1)$. This result is 1.8 standard deviations from the conjectured value.

The tricritical one-state Potts model corresponds to $g = 4/3$, and $\tau = 379/187$, and conjecture (14) yields $\Omega = 72/187 \approx 0.385027$. Since the tricritical one-state Potts model belongs to the same universality class as the usual Ising model, it exhibits a rich symmetry and rather strong finite-size effects. Fig. 6(c) shows that the data for different system sizes differ significantly. However, after excluding the effects from small and large s , a linear trend is still observed. Unfortunately, the power-law fit to the Ansatz (49) is more challenging. Even if we consider only the data for $L = 2048$, we could only achieve a stable fit by choosing $s_{\max} = 64$, as reported in Table II. We obtain $\Omega = 0.37(1)$, which is 1.5 standard deviations from the conjectured value.

VI. DISCUSSION

We have studied the cluster-size distribution n_s (1) for the two-dimensional $O(n)$ loop model (17) on the branches x_\pm (18) for $n \in [1, 2]$. On both branches, the $O(n)$ loop model can be represented as a Coulomb gas with a certain coupling constant $g \in [1/2, 2]$. Furthermore, on x_+ the $O(n)$ loop model is critical, and it belongs to the same universality class as the tricritical Potts model with $Q = n^2$ states. This model has a Coulomb-gas representation with $g \in [1, 2]$. In addition, the branch x_- is in the dense critical phase of the $O(n)$ loop model. This phase belongs to the same universality class as the critical Potts model with $Q = n^2$ states. This model has a Coulomb-gas representation with $g \in [1/2, 1]$. The goal of this article was to gain new insights about the correction-to-scaling exponent Ω in (1).

First, we have obtained a closed-form expression for Ω as a function of g [cf. (14)] by starting from Cardy's result on the partition function of the $O(n)$ model on this annulus [57], and generalizing an argument by Ziff [4]. The result is, not surprisingly, a rational function of g , and indeed it gives the exact result for percolation obtained by Ziff.

We have then confirmed the validity of conjecture (14) by performing high-precision Monte Carlo simulations. We have chosen to simulate the $O(n)$ loop model rather than the critical or tricritical Potts models. There are two main motivations to do so: (1) critical slowing down is absent on x_- , and is moderate for $Q \in [1, 2]$ on x_+ ; and (2) the leading exponents are absent in the $O(n)$ model.

This implies that the effect of the higher-order terms not included in the Ansatz (49) are smaller than expected. We have applied a cluster Monte Carlo algorithm to a generalized Ising model (45) which is equivalent (modulo boundary conditions) to the $O(n)$ loop model.

The numerical results fully support conjecture (14) for Ω when $Q = 1, 2, 3$ on the x_- branch, $Q = 1, 2$ on the x_+ branch, and $Q = 4$, which belongs to both branches. In the description of the fit results (Section V), it is frequently mentioned that there exists some deviations (up to two error bars) between the numerical estimate and the theoretical prediction. We emphasize that this is a typical phenomenon since potential systematic errors are not taken sufficiently into account in the analyses, which would in principle need a careful extrapolation for both the $s \rightarrow \infty$ and the $L \rightarrow \infty$ limits.

We believe that the conjecture for Ω extends to the whole branches x_{\pm} . This means the interval $Q \in [0, 4]$ for both the critical and tricritical Potts models, and the interval $n \in [-2, 2]$ for the $O(n)$ loop model. Additional Monte Carlo simulations could be done to see whether

this conjecture is true.

It is also worth noticing that the difference between the two most relevant magnetic eigenvalues $y_{h1} - y_{h2}$ is related to the exponent Ω (i.e., $y_{h1} - y_{h2} = \Omega d_f = \Omega y_{h1}$). This means that it is possible to obtain the subleading magnetic exponent by measuring Ω in e.g., d -dimensional percolation. This observation could be useful to obtain accurate results for the subleading exponent y_{h2} in other models.

ACKNOWLEDGMENTS

We thank Robert M. Ziff for fruitful discussions. This work has been supported by the National Natural Science Foundation of China (under Grant No. 12275263), the Innovation Program for Quantum Science and Technology (under grant No. 2021ZD0301900), the Natural Science Foundation of Fujian Province of China (under Grant No. 2023J02032).

-
- [1] D. Stauffer and A. Aharony, *Introduction to Percolation Theory*, 2nd ed. (Taylor and Francis, London, 1994).
 - [2] B. Bollobás and O. Riordan, *Percolation* (Cambridge University Press, Cambridge, 2006).
 - [3] J. Adler, M. Moshe, and V. Privman, New method for analyzing confluent singularities and its application to two-dimensional percolation, *Phys. Rev. B* **26**, 1411 (1982).
 - [4] R. M. Ziff, Correction-to-scaling exponent for two-dimensional percolation, *Phys. Rev. E* **83**, 020107(R) (2011), [arXiv:1101.0807](#).
 - [5] R. M. Ziff and F. Babalievski, Site percolation on the Penrose rhomb lattice, *Physica A* **269**, 201 (1999), [arXiv:1101.0807](#).
 - [6] A. Aharony and J. Asikainen, Fractal dimensions and corrections to scaling for critical Potts clusters, *Fractals* **11**, 3 (2003), [arXiv:cond-mat/0206367](#).
 - [7] P. Di Francesco, P. Mathieu, and M. Sénéchal, *Conformal Field Theory* (Springer-Verlag, New York, 1997).
 - [8] G. Grimmett, *The Random-Cluster Model* (Springer, Heidelberg, 2006).
 - [9] R. B. Potts, Some generalized order-disorder transformations, *Proc. Cambridge Philos. Soc.* **48**, 106 (1952).
 - [10] F. Y. Wu, The Potts model, *Rev. Mod. Phys.* **54**, 235 (1982).
 - [11] F. Y. Wu, Erratum: The Potts model, *Rev. Mod. Phys.* **55**, 315 (1983).
 - [12] F. Y. Wu, Potts model of magnetism (invited), *J. Appl. Phys.* **55**, 2421 (1984).
 - [13] R. J. Baxter, *Exactly Solved Models in Statistical Mechanics* (World Scientific, Singapore, 1985).
 - [14] P. W. Kasteleyn and C. M. Fortuin, Phase transitions in lattice systems with random local properties, *J. Phys. Soc. Jpn. Suppl.* **26**, 11 (1969).
 - [15] C. M. Fortuin and P. W. Kasteleyn, On the random-cluster model: I. Introduction and relation to other models, *Physica* **57**, 536 (1972).
 - [16] B. Nienhuis, A. N. Berker, E. K. Riedel, and M. Schick, First- and Second-Order Phase Transitions in Potts Models: Renormalization-Group Solution, *Phys. Rev. Lett.* **43**, 737 (1979).
 - [17] B. Nienhuis, E. K. Riedel, and M. Schick, Variational renormalisation-group approach to the q -state Potts model in two dimensions, *J. Phys. A: Math. Gen.* **13**, L31 (1980).
 - [18] K. K. Murata, Hamiltonian formulation of site percolation in a lattice gas, *J. Phys. A: Math. Gen.* **12**, 81 (1979).
 - [19] B. Nienhuis, Analytical calculation of two leading exponents of the dilute Potts model, *J. Phys. A: Math. Gen.* **15**, 199 (1982).
 - [20] W. Janke and M. J. Schakel, Geometrical vs. Fortuin-Kasteleyn clusters in the two-dimensional q -state Potts model, *Nucl. Phys. B* **700**, 385 (2004), [arXiv:cond-mat/0311624](#).
 - [21] Y. Deng, J. R. Heringa, and H. W. J. Blöte, Constrained tricritical phenomena in two dimensions, *Phys. Rev. E* **71**, 036115 (2005).
 - [22] X. Qian, Y. Deng, and H. W. J. Blöte, Dilute Potts model in two dimensions, *Phys. Rev. E* **72**, 056132 (2005).
 - [23] B. Nienhuis and M. Nauenberg, First-Order Phase Transitions in Renormalization-Group Theory, *Phys. Rev. Lett.* **45**, 777 (1975).
 - [24] W. Klein, D. J. Wallace, and P. K. P. Zia, Essential Singularities at First-Order Phase Transitions, *Phys. Rev. Lett.* **37**, 639 (1976).
 - [25] M. E. Fisher and N. H. Berker, Scaling for first-order transitions in thermodynamic and finite systems, *Phys. Rev. B* **26**, 2507 (1978).
 - [26] B. Nienhuis, Critical behavior of two-dimensional spin models and charge asymmetry in the Coulomb gas, *J. Stat. Phys.* **34**, 731 (1984).
 - [27] B. Nienhuis, Coulomb gas formulations of two-dimensional phase transitions, in *Phase transitions and critical phenomena*, Vol. 11, edited by C. Domb and J. L.

- Lebowitz (Academic Press, London, 1987) pp. 1–53.
- [28] M. Nauenberg and D. J. Scalapino, Singularities and Scaling Functions at the Potts-Model Multicritical Point, *Phys. Rev. Lett.* **44**, 837 (1980).
- [29] J. L. Cardy, M. Nauenberg, and D. J. Scalapino, Macroscopic loops in the loop $O(n)$ model at Nienhuis' critical point, *Phys. Rev. B* **22**, 2560 (1980).
- [30] J. Salas and A. D. Sokal, Logarithmic Corrections and Finite-Size Scaling in the Two-Dimensional 4-State Potts Model, *J. Stat. Phys.* **88**, 567 (1997), [arXiv:hep-lat/9607030](#).
- [31] H. Saleur and B. Duplantier, Exact Determination of the Percolation Hull Exponent in Two Dimension, *Phys. Rev. Lett.* **58**, 2325 (1987).
- [32] P. Nolin, W. Qian, X. Sun, and Z. Zhuang, Backbone exponent for two-dimensional percolation, [arXiv:2309.05050](#) (2023), preprint.
- [33] D. P. Landau and K. Binder, *A Guide to Monte-Carlo Simulations in Statistical Physics*, 4th ed. (Cambridge University Press, Cambridge, 2014).
- [34] A. D. Sokal, Monte Carlo Methods in Statistical Mechanics: Foundations and New Algorithms, in *Functional Integration: Basics and Applications*, edited by C. DeWitt-Morette, P. Cartier, and A. Folacci (Plenum, New York, 1997) pp. 131–192.
- [35] R. H. Swendsen and J.-S. Wang, Nonuniversal Critical Dynamics in Monte Carlo Simulations, *Phys. Rev. Lett.* **58**, 86 (1987).
- [36] X.-J. Li and A. D. Sokal, Rigorous lower bound on the dynamic critical exponent of the Swendsen–Wang algorithm, *Phys. Rev. Lett.* **63**, 827 (1989).
- [37] L. Chayes and J. Machta, Graphical representations and cluster algorithms II, *Physica A* **254**, 477 (1998).
- [38] Y. Deng, T. M. Garoni, J. Machta, G. Ossola, G. Poin, and A. D. Sokal, Critical Behavior of the Chayes–Machta–Swendsen–Wang Dynamics, *Phys. Rev. Lett.* **99**, 055701 (2007), [arXiv:0705.2751](#).
- [39] N. Prokof'ev and B. Svistunov, Worm Algorithms for Classical Statistical Models, *Phys. Rev. Lett.* **87**, 160601 (2001), [arXiv:cond-mat/0103146](#).
- [40] Y. Deng, T. Garoni, and A. D. Sokal, Dynamic critical behavior of the worm algorithm for the Ising model, *Phys. Rev. Lett.* **99**, 110601 (2007), [arXiv:cond-mat/0703787](#).
- [41] J. Salas and A. D. Sokal, Universal amplitude ratios in the critical two-dimensional Ising model on a torus, *J. Stat. Phys.* **98**, 551 (2000), The relevant part is contained in the first preprint version of this paper, [arXiv:cond-mat/9904038v1](#).
- [42] B. Nienhuis, Exact Critical Point and Critical Exponents of $O(n)$ Models in Two Dimensions, *Phys. Rev. Lett.* **49**, 1062 (1982).
- [43] M. Batchelor and H. W. J. Blöte, Conformal invariance and critical behavior of the $O(n)$ model on the honeycomb lattice, *Phys. Rev. B* **39**, 2391 (1989).
- [44] R. Peled and Y. Spinka, Lectures on the Spin and Loop $O(n)$ Models, in *Sojourns in Probability Theory and Statistical Physics - I. Spin Glasses and Statistical Mechanics, A Festschrift for Charles M. Newman*, Springer Proceedings in Mathematics & Statistics, Vol. 298, edited by V. Sidoravicius (Springer Nature Singapore, 2019) pp. 246–320, [arXiv:1708.00058](#).
- [45] H. Duminil-Copin, A. Glazman, R. Peled, and Y. Spinka, Macroscopic loops in the loop $O(n)$ model at Nienhuis' critical point, *J. Eur. Math. Soc.* **23**, 315 (2021), [arXiv:1707.09335](#).
- [46] R. J. Baxter, q colourings of the triangular lattice, *J. Phys. A: Math. Gen.* **19**, 2821 (1986).
- [47] R. J. Baxter, Chromatic polynomials of large triangular lattices, *J. Phys. A: Math. Gen.* **20**, 5241 (1987).
- [48] Y. Deng, T. M. Garoni, W. Guo, H. W. J. Blöte, and A. D. Sokal, Cluster Simulations of Loop Models on Two-Dimensional Lattices, *Phys. Rev. Lett.* **98**, 120601 (2007).
- [49] C. Ding, X. Qian, Y. Deng, W. Guo, and H. W. K. Blöte, Geometric properties of two-dimensional $O(n)$ loop configurations, *J. Phys. A: Math. Theor.* **40**, 3305 (2007), [arXiv:cond-mat/0608547](#).
- [50] Q. Liu, Y. Deng, and T. Garoni, Worm Monte Carlo study of the honeycomb-lattice loop model, *Nucl. Phys. B* **846**, 283 (2011), [arXiv:1011.1980](#).
- [51] S. Fang, D. Ke, W. Zhong, and Y. Deng, Backbone and shortest-path exponents of the two-dimensional Q -state Potts model, *Phys. Rev. E* **105**, 044122 (2022), [arXiv:2112.10162](#).
- [52] J. L. Cardy, Conformal invariance, in *Phase transitions and critical phenomena*, Vol. 11, edited by C. Domb and J. L. Lebowitz (Academic Press, London, 1987) pp. 55–126.
- [53] H. Duminil-Copin and S. Smirnov, The connective constant of the honeycomb lattice equals $\sqrt{2 + \sqrt{2}}$, *Ann. Math.* **175**, 1653 (2012), [arXiv:1007.0575](#).
- [54] H. W. J. Blöte and B. Nienhuis, Fully packed loop model on the honeycomb lattice, *Phys. Rev. Lett.* **72**, 1372 (1994).
- [55] M. Batchelor, J. Suzuki, and C. M. Yung, Exact results for Hamiltonian walks from the solution of the fully packed loop model on the honeycomb lattice, *Phys. Rev. Lett.* **73**, 2646 (1994).
- [56] J. Kondev, J. de Gier, and B. Nienhuis, Operator spectrum and exact exponents of the fully packed loop model, *J. Phys. A: Math. Gen.* **29**, 6489 (1996), [arXiv:cond-mat/9603170](#).
- [57] J. L. Cardy, The $O(n)$ Model on the Annulus, *J. Stat. Phys.* **125**, 1 (2006), [arXiv:math-ph/0604043](#).
- [58] Y. Deng, W. Guo, and H. W. J. Blöte, Cluster Simulation of the $O(N)$ loop model on the Honeycomb lattice, [arXiv:cond-mat/0608447](#) (2006), preprint.
- [59] Please note that the Ising model is *not* written as a 2-state Potts model (3)/(4). We use instead the standard Ising model notation given by (45).